Icarus **157**, 476–489 (2002)
doi:10.1006/icar.2002.6821

The Dual Sources of Io's Sodium Clouds

Jody K. Wilson, Michael Mendillo, and Jeffrey Baumgardner

Center for Space Physics, Boston University, 725 Commonwealth Avenue, Boston, Massachusetts 02215
E-mail: jkwilson@bu.edu

Nicholas M. Schneider

Laboratory for Atmospheric and Space Physics, University of Colorado, Boulder, Colorado 80309-0392

John T. Trauger

Jet Propulsion Laboratory/Caltech, MS 179-225, 4800 Oak Grove Drive, Pasadena, California 91109

and

Brian Flynn

Space Sciences Laboratory, University of California, Berkeley, California 94720-7450

Received February 19, 1999; revised December 19, 2001

Io's sodium clouds result mostly from a combination of two atmospheric escape processes at Io. Neutralization of Na^+ and/or NaX^+ pickup ions produces the "stream" and the "jet" and results in a rectangular-shaped sodium nebula around Jupiter. Atmospheric sputtering of Na by plasma torus ions produces the "banana cloud" near Io and a diamond-shaped sodium nebula. Charge exchange of thermal Na^+ with Na in Io's atmosphere does not appear to be a major atmospheric ejection process. The total ejection rate of sodium from Io varied from 3×10^{26} to 25×10^{26} atoms/s over seven years of observations. Our results provide further evidence that Io's atmospheric escape is driven from collisionally thick regions of the atmosphere rather than from the exosphere.

Key Words: **Io; atmospheric dynamics; satellite atmospheres; magnetospheres.**

INTRODUCTION

For over two decades, researchers have been observing the morphology and dynamics of Io's neutral sodium clouds to better understand the complex interaction between Io's atmosphere and Jupiter's powerful magnetosphere. Io's volcanically generated SO_2 atmosphere is constantly being lost to space by means of several ejection processes. In Io's atmosphere, solar ultraviolet photons and magnetospheric electrons ionize atoms and molecules and these ions are then picked up and incorporated into the magnetically confined plasma torus encircling Jupiter. These heavy ions in the torus in turn collide with neutrals in Io's atmosphere, either ejecting them from Io via elastic collisions or ionizing them by charge exchange collisions. Molecules and atoms which are ejected as neutrals form extended neutral clouds around Io and Jupiter, and the morphology of each cloud component is a reflection of the atmospheric ejection mechanism which generates it.

The neutral clouds of sodium are particularly useful for studying the Io–magnetosphere system. Atomic sodium (Na) is only a trace constituent of the atmosphere (∼few %), but its large cross section for scattering visible sunlight makes it by far the most easily observed species in the neutral clouds. The Na clouds are thus a convenient means of indirectly observing the instantaneous supply of plasma to the plasma torus. Figure 1 shows the basic morphologies of the sodium clouds from three different perspectives. The Na "banana" cloud and similar clouds of sulfur and oxygen species are eroded by ionization, adding mass to the torus. The molecular ion "stream" results from ionization and pickup of sodium-bearing molecules directly from Io's atmosphere, perhaps paralleling other molecules of sulfur and oxygen. A broad review of Io, its atmosphere, and extended neutral clouds can be found in Spencer and Schneider (1996).

Sodium cloud imaging observations have generally been conducted at two widely disparate fields of view (FOVs). Most of the data on Io's Na cloud features come from observations similar to those shown in Fig. 1 (middle panel), spanning 15 jovian radii (R_J) or less. Models have been developed to study the source mechanisms that produce the various observed cloud components. The mechanisms include atmospheric sputtering for the banana cloud (Smyth and Combi 1988), pickup ion neutralization in Io's atmosphere for the jet (Wilson and Schneider 1999,

0019-1035/02 $35.00

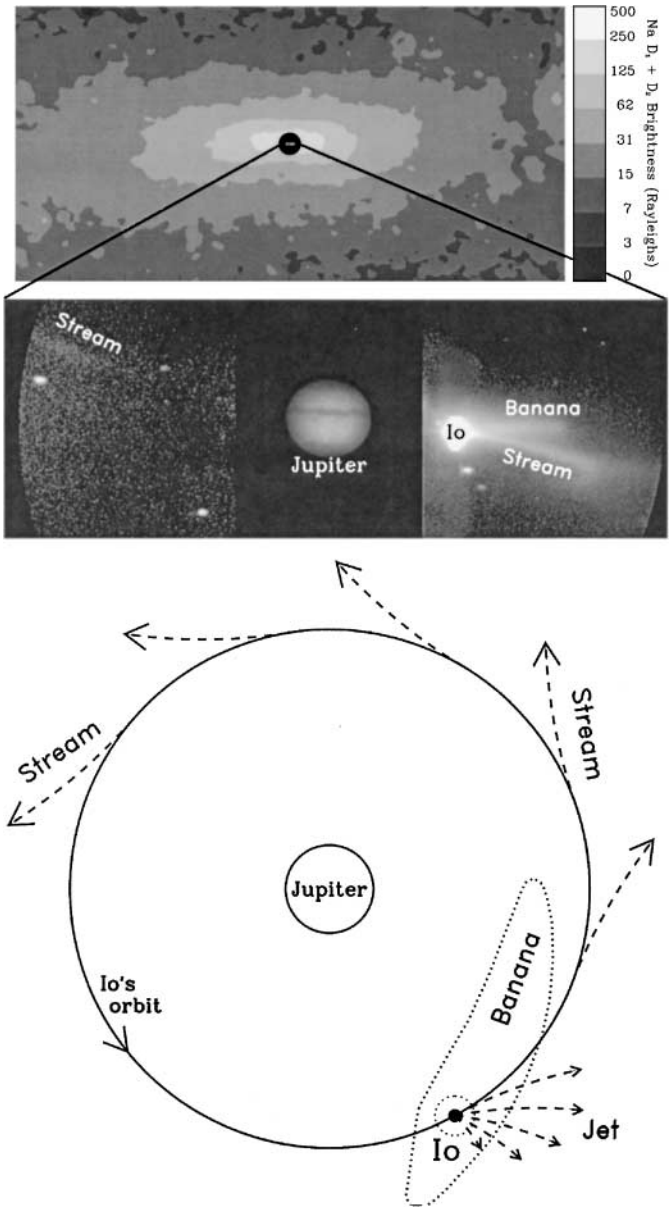

FIG. 1. Sodium clouds. (Top) Large FOV image showing the sodium nebula on July 21, 1995. This is the brightest sodium nebula in this data set. (Middle) Small FOV image of Io sodium clouds, taken on January 12, 1990, from the Catalina Observatory. (Bottom) Diagram of same geometry viewed from over Jupiter's north pole. Arrows indicate fast sodium trajectories. Labeled cloud features are the "banana cloud," which orbits Jupiter and which is composed of Na atoms ejected at low speeds (∼few km/s) from Io by atmospheric sputtering; the molecular ion "stream," composed of fast sodium atoms which are ejected from the torus by dissociation or dissociative recombination of unidentified molecular pickup ions containing sodium (NaX^+); and the "jet," produced by pickup ion neutralization in Io's atmosphere.

Burger *et al*. 1999), molecular pickup ion destruction in the torus for the stream (Schneider *et al*. 1991, Wilson and Schneider 1994), and specific exobase velocity distributions for the near-Io corona (Smyth and Combi 1997).

Images of Na emission spanning a much larger FOV (up to 1000 R_J) portray the ultimate distribution of the "fast" Na atoms ($v > 10$ km/s) leaving the system (Mendillo *et al*. 1990, Flynn *et al*. 1992, 1994). The morphology of this "sodium nebula" has been explained with yet another process, charge exchange of thermal Na^+ torus ions in Io's exosphere (Mendillo *et al*. 1990, Smyth and Combi 1991, Flynn *et al*. 1992), although Flynn (1993) demonstrated that the molecular ion stream could produce the observed nebula under certain conditions. The top panel of Fig. 1 shows one of the brightest apparitions of the sodium nebula.

Here we present Na data images covering three fields of view, including a new intermediate FOV spanning 70 R_J. We apply models simultaneously to all three FOVs to provide new constraints on Io's atmospheric escape processes.

OBSERVATIONS

Figure 2 shows the data images used in this paper. The large and medium FOV observations (Tables I and II) were made at the Boston University Station at McDonald Observatory, with the exception of the 1992 observations, which were made from Mt. Haleakala on the island of Maui. All observations used narrow-band interference filters and occulting masks to block light from Jupiter. Images were taken at two wavelengths: one near the Na D-line wavelengths of 5890 and 5896 Å, and one at an off-band wavelength for measuring terrestrial atmospheric and instrumental scattered light. The images shown are the result of subtracting the off-band images from the Na images, so that only Na emission remains. The large FOV images were taken with a 0.1-m refracting telescope and an intensified CCD camera (Baumgardner *et al*. 1993). The medium FOV images were taken with a 0.5-m Ritchey–Chretien telescope and a CCD camera (Mendillo *et al*. 1997). For 1992 and 1993, when the nebula was particularly dim, several images from different times have been co-added to increase the signal-to-noise ratio. This would smear out any longitudinal variations in the nebula; typically, however,

TABLE I
Large FOV Observations

Date	UT	λ_{III}(CML)[a]	λ_{III}(Io)[b]	θ_{Io}[c]	Sub-Earth latitude
1990 Jan. 25	2:54	354°	229°	305°	+2.4°
1991 Feb. 7	9:08	208°	186°	202°	+0.4°
1992 Feb. 6–8	(multiple)	—	—	—	−1.7°
1993 Mar. 19–20	(multiple)	—	—	—	−3.2°
1994 July 12	3:45	322°	29°	113°	−3.5°
1995 July 21	3:42	72°	25°	227°	−3.3°
1996 Sept. 30	1:50	233°	231°	182°	−1.9°

[a] System-III (magnetic) longitude of Jupiter's central meridian.
[b] System-III longitude of Io.
[c] Orbital longitude of Io.

TABLE II
Medium FOV Observations

Date	UT	λ_{III}(CML)	λ_{III}(Io)	θ_{Io}	Sub-Earth latitude
1994 July 18	3:55	151°	76°	255°	−3.4°
1995 July 21	4:00	83°	33°	230°	−3.3°
1996 Sept. 30	3:05	279°	266°	193°	−1.9°

there are no such changes on a day-to-day basis (Mendillo *et al*. 1992, Flynn *et al*. 1994).

The Na nebulas seen in the large FOV images vary between two subtle shapes. In 1991, 1992, and 1995 the brightness contours of the nebula had a rectangular shape, while the 1994 and 1996 nebulas are best described as diamond-shaped. Other nebulas appear to be intermediate in shape. The three images at the medium FOV are characterized by emission with concentric and symmetrical brightness contours. The 1995 medium FOV image is much brighter than those in 1994 and 1996, in agreement with the large FOV images, and also shows a jet extending from Io.

The small FOV observations (Table III) were conducted at the Catalina Observatory 1.5-m telescope (1990–1992), the Las Campanas Observatory 2.5-m telescope (1994), the Apache Point Observatory 3.5-m telescope (1995), and the Mt. Wilson Observatory 2.5-m telescope (1996). Each observation used a CCD detector, narrow-band sodium filters, and neutral-density filters to reduce the brightness of the image of Jupiter. Data were reduced and analyzed as described in Schneider and Trauger (1995). The images are not calibrated for absolute brightness. The 1996 small FOV data have a lower signal-to-noise ratio due to greater scattered light. To make the narrow features more visible, all small FOV images are shown in gray scale. Three features appear in various combinations in the small FOV images. The banana cloud is visible in all images except for the 1995 image. The stream is visible in 1990 and 1991, and the jet is the only obvious feature in 1995. These processes are described more fully in a later section.

The brightness and morphologies of the sodium clouds changed significantly between the various observations shown here, indicating changes in both the total escape rate of Na and in the relative importance of specific escape processes. We use a model of Na ejection from Io's atmosphere to characterize the atmospheric escape from Io and to determine the relationship between the features seen in the different fields of view. We assume that the Na clouds and associated atmospheric ejection processes did not change between the observations taken during the same year, and we therefore use the same model for each FOV in a given year. This is a strong assumption for the 1995 and 1996 data, in which the small FOV observations are displaced 2–3 months from the other images; however, in the final analysis, this appears to be an adequate assumption for these particular cases.

MODEL DESCRIPTION

We simulate the sodium clouds with a numerical Monte Carlo model of sodium atom ejection from Io and from the torus. Atoms are given ejection speeds and directions that are randomized within certain constraints that are determined by the ejection mechanism. Orbits are calculated using fourth-order Runge–Kutta integration and include the effects of Io's gravity and Jupiter's gravity. The simulated emission by resonant scattering of sunlight includes the effects of both the solar Fraunhofer absorption features at the D-line wavelengths and the Doppler shift of the resonant scattering wavelengths due to the atoms' radial heliocentric velocities.

We simulate electron impact ionization by using a simplified version of the lifetime spatial distribution calculated by Smyth and Combi (1988). The distribution used in our model is shown in Fig. 3. We center this distribution on the plasma torus latitude for all longitudes, using the torus "ribbon" latitudes found by Schneider and Trauger (1995). Electron impact ionization is particularly important for atoms in orbits which spend several hours or more between 5 and 10 R_J from Jupiter, where ionization rates are highest.

The sodium photoionization lifetime we use (1200 h at Jupiter) is longer than the experimentally derived value (400 h) adopted by other Io sodium cloud modelers (Smyth and Combi 1991, Flynn *et al*. 1992). Theoretical calculations of the sodium photoionization cross section of sodium atoms correspond to a lifetime of 45 h at 1 AU (Huebner *et al*. 1992), or 1200 h at Jupiter's orbital distance of 5.2 AU. Some recent studies of sodium in comets seem to indicate that this longer value is correct (Combi *et al*. 1997, Cremonese *et al*. 1997). The major effect of the

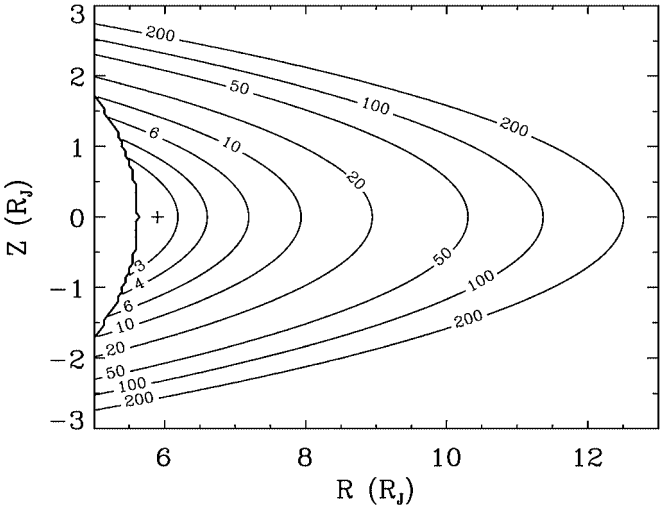

FIG. 3. Electron impact ionization lifetime of Na used in the model, plotted in a meridianal plane. Contours are labeled with the lifetime in hours. The cross (+) indicates Io's orbital distance at the magnetic equator of Jupiter. Jupiter's plasma torus is tilted by ∼7° relative to Jupiter's rotational axis, so Io usually lies north or south of this point.

TABLE III
Small FOV Observations

Date	UT	λ_{III}(CML)[a]	λ_{III}(Io)[b]	θ_{Io}[c]	Sub-Earth latitude
1990 Jan. 10	9:10	122°	126°	176°	+2.4°
1991 Feb. 6	4:47	260°	118°	322°	+0.4°
1992 Feb. 9	11:43	73°	263°	350°	−1.7°
1994 July 25	3:23	104°	50°	234°	−3.4°
1995 May 8	7:40	230°	95°	315°	−3.5°
1996 June 22	6:51	120°	269°	31°	−2.0°

[a] System-III (magnetic) longitude of Jupiter's central meridian.
[b] System-III longitude of Io.
[c] Orbital longitude of Io.

longer lifetime in our model is to allow sodium atoms to travel further from Jupiter before being photoionized. This allows lower speed Na atoms to contribute more to the distant regions of the nebula seen in the large FOV images.

We generate model images by calculating the positions and velocities of the sodium atoms in three dimensions and then calculating the emission from each model particle and adding it to the two-dimensional image array. To save computation time we use models for a limited number of Io magnetic longitudes (29°, 50°, 76°, 95°, 122°, 186°, 230°, 266°), which together represent all of the Io magnetic longitudes in the data to within 4° (see Tables I–III). These geometries only require the proper rotation around Jupiter to match Io's orbital longitude in each data image. This means that we cannot include radiation pressure in our model since its direction relative to Io depends on Io's orbital longitude; however, with the exception of subtle changes in the banana cloud (Smyth and Combi 1988), the effects of radiation pressure on the sodium clouds at Jupiter are not significant for the broad analysis and spatial scales we are using. Sodium atoms escaping from Jupiter are accelerated away from the Sun, or essentially away from the Earth, meaning that their locations as seen from the Earth are minimally affected. Table IV lists the relevant parameters for each atmospheric escape model, and further details of each process are given in the next section.

PROCESS DESCRIPTIONS AND MODELING RESULTS

Figures 4–6 present model images of the Na clouds generated by the various atmospheric ejection processes. For each escape process, we generate images covering the same three FOVs as the data (15, 70, and 1000 R_J across, respectively). The geometries are not the same between different FOVs in the same year, so certain features appear differently from one field of view to the next, even though all other aspects of the model are identical. As with the data images, small FOV model images are shown in gray scale. The portion of the 1995 medium FOV image showing the jet is also displayed in gray scale in the model images.

Pickup ion neutralization: The stream. The molecular ion stream, which appears intermittently, is created by a two-step process: (1) molecular ions containing sodium (NaX^+) are created at Io and picked up by the plasma torus; (2) hours later and far from Io each ion eventually collides with an electron and undergoes one of three reactions, at least two of which yield neutral high-speed sodium (Na_{fast}):

$$NaX^+_{pickup} + e^- \rightarrow Na_{fast} + X_{fast} \quad \text{(dissociative recombination)} \quad (1a)$$

$$\rightarrow Na_{fast} + X^+ + e^- \quad \text{(dissociation)} \quad (1b)$$

$$\rightarrow Na^+ + X_{fast} + e^- \quad \text{(dissociation)} \quad (1c)$$

(Schneider *et al*. 1991). The identity of "X" is unknown but may include one or more atoms of O, S, Na (e.g., Johnson 1994a), and Cl (Küppers and Schneider 2000, Moses *et al*. 2000). NaX^+ has not been detected yet, and its presence is inferred only by the daughter Na_{fast} atoms ejected from the torus. The branching ratios of these reactions are also uncertain, so the observed Na_{fast} ejection rate from the torus is an unknown fraction of the rate of NaX^+ escape from Io. Possible sources of NaX^+ at Io include photoionization of NaX, electron impact ionization of NaX, and reactions of atmospheric Na with molecular ion species (e.g., SO_2^+, Johnson 1994a).

The daughter Na atoms are ejected from a broad region in the torus, the morphology of which is determined by the motions

TABLE IV
Summary of Model Parameters

Process	Fixed parameters	Free parameters
Thermal exospheric charge exchange	• Plasma temperature (50 eV) • Dual plasma drift speeds (37 + 74 km/s)	• Ejection rate of Na
Stream	• B-field direction vs longitude	• Ejection rate of Na • V_{pickup} (10, 30, 60 km/s) • Initial pitch angle distribution of ions • Lifetime of NaX^+ (3–10 h)
Jet	• B-field direction vs longitude • Location of Na ejection (antijovian hemisphere)	• Ejection rate of Na • V_{pickup} (10, 30, 60 km/s) • Initial pitch angle distribution of ions
Atmospheric sputtering	• Ejection direction (isotropic)	• Ejection rate of Na • Speed distribution (from Smyth and Combi 1988)
Pilcher *et al.* "Directional Feature"	• Velocity distribution (20 km/s ⊥ to Io's motion)	• Ejection rate of Na

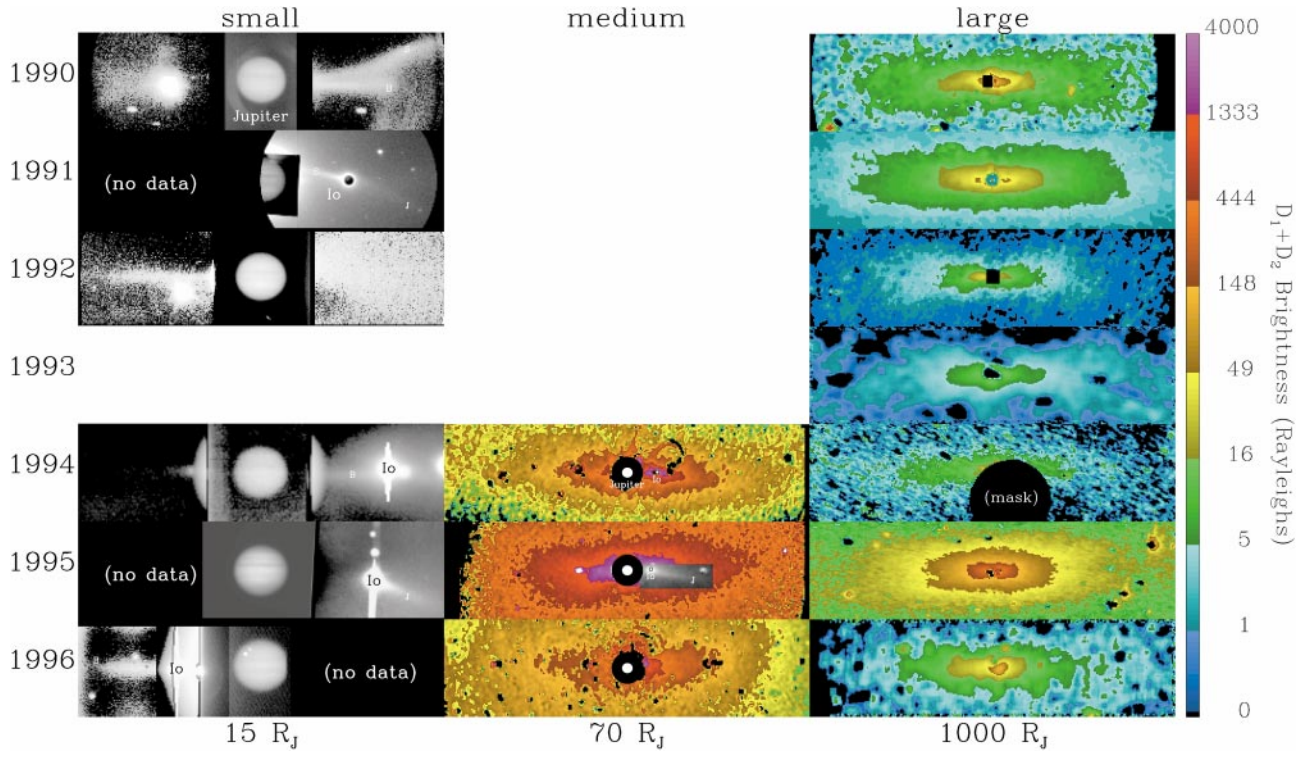

FIG. 2. Data images of the sodium clouds. (Left column) Small FOV spanning 15 R_J. (Middle column). Medium FOV spanning 70 R_J. (Right column) Large FOV spanning 1000 R_J. Jupiter is at the center of each image. The banana cloud ('B'), jet ('J'), and stream ('S') are labeled in the small FOV images. Small FOV images are not calibrated for absolute brightness, so relative brightness above the background nebula brightness is indicated in gray scale, with each year scaled according to the intrinsic brightness of the Na. Note that Io saturates a region in the small FOV images that is much larger than Io itself and that an occulting mask was placed over Io in the 1991 image. A larger occulting mask for lunar observations was used in the 1994 large FOV image, obscuring much of the central region of the Na nebula. In the 1995 medium FOV, a region of the image is displayed in gray scale to highlight the jet. Circles indicating Io's location in the medium FOV are not drawn to scale.

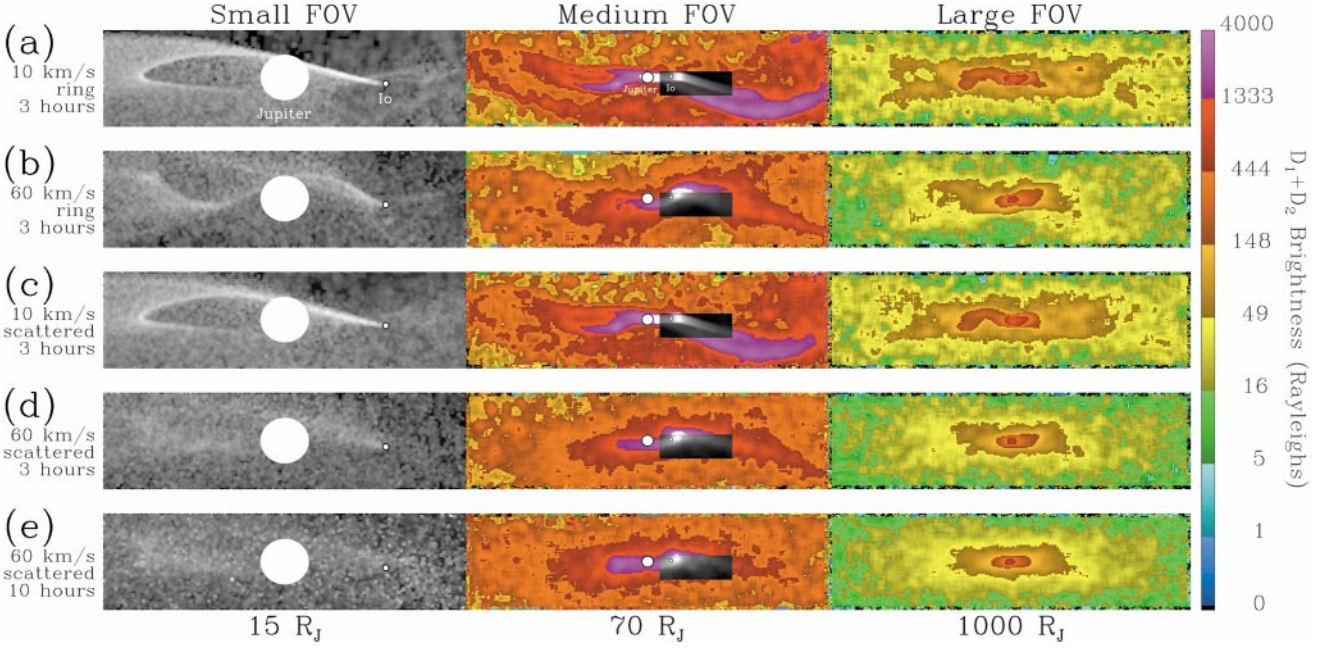

FIG. 4. Stream model images for the geometries of the 1995 data, using an escape rate of 2.5×10^{27} Na atoms/s. The fields of view are 15, 70, and 1000 R_J from left to right. (a) Parent pickup ions in 10 km/s ring distribution and with lifetime of 3 h. (b) 60 km/s ring distribution and 3-h lifetime. (c) 10 km/s scattered distribution and 3-h lifetime. (d) 60 km/s scattered distribution and 3-h lifetime. (e) 60 km/s scattered distribution and 10-h lifetime. Note that Io is not drawn to scale.

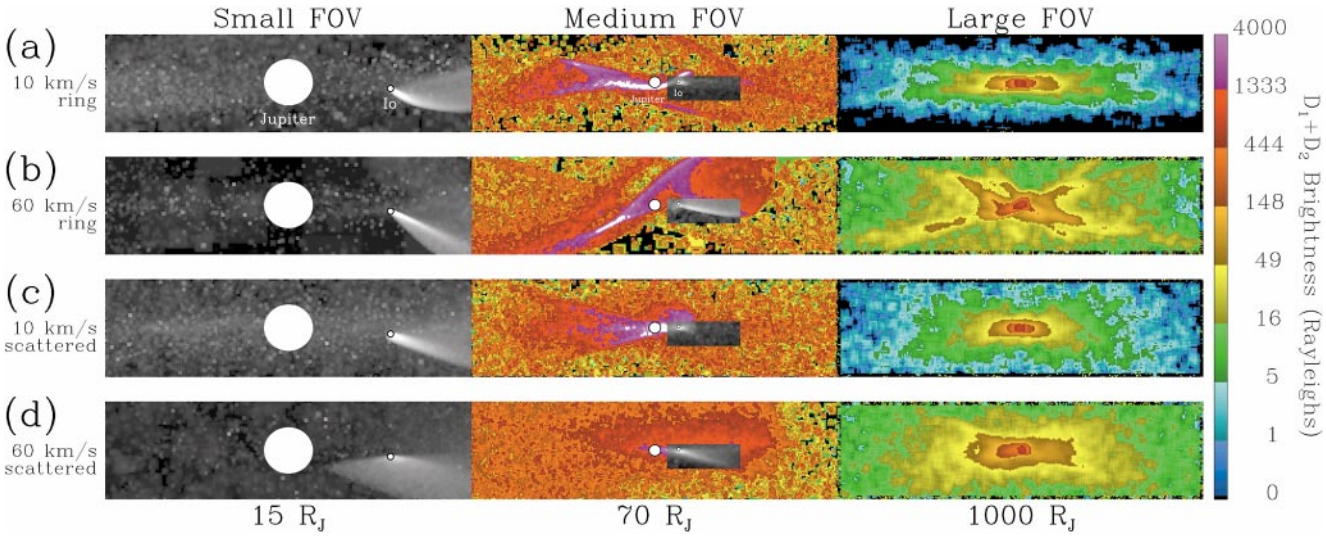

FIG. 5. Jet model images for geometries of the 1995 data, using an escape rate of 1.5×10^{27} Na atoms/s. The fields of view are 15, 70, and 1000 R_J from left to right. (a) Parent pickup ions in 10 km/s ring distribution. (b) 60 km/s ring distribution. (c) 10 km/s scattered distribution. (d) 60 km/s scattered distribution.

of the NaX^+ pickup ions. The velocities of the ejected atoms are a combination of the magnetospheric rotation speed near Io's orbit (~74 km/s) and the ion gyromotion (<60 km/s) and bounce motion (<12 km/s) around and along magnetic field lines (Wilson and Schneider 1994). Since the ions bounce along field lines, the sodium source region in the torus at any given longitude moves north and south over the course of several hours.

The free parameters for this model are (1) the ejection rate of Na from pickup ion neutralization, (2) the pickup speed, (3) the velocity modification of the parent ions, and (4) the total lifetime of the pickup ions in the torus. We model pickup speeds of between 10 and 60 km/s (57 km/s is the magnetospheric corotation speed relative to Io), lifetimes of 3 to 10 h, and Na ejection rates of order 10^{26} to 10^{27} atoms/s.

We use two cases for velocity modification of the parent pickup ions. The first case is no modification, resulting in a so-called ring distribution with the gyrospeed equal to the pickup speed. In the second case, Gaussian distributions are used for both the gyrospeeds and initial parallel (to **B**) velocities of the parent ions; this approximates the effects of either pickup followed by collisions in Io's atmosphere (Wilson 1996) or pitch-angle scattering by plasma waves.

Figure 4 shows five model simulations of the stream for the same geometries as the 1995 data and with a Na ejection rate of 2.5×10^{27} atoms/s. Lower gyrospeeds (10 km/s, Figs. 4a and 4c) yield an obvious narrow stream feature in the small and medium FOVs and asymmetric and "blotchy" nebulas in the medium and large FOVs. For the same lifetime, higher gyrospeeds (60 km/s, Figs. 4b and 4d) result in a less distinct stream and a smoother, more symmetrical nebula. Similarly, the ring distribution (Figs. 4a and 4b) yields a more obvious stream feature and slightly less uniform nebula compared to the scattered distribution

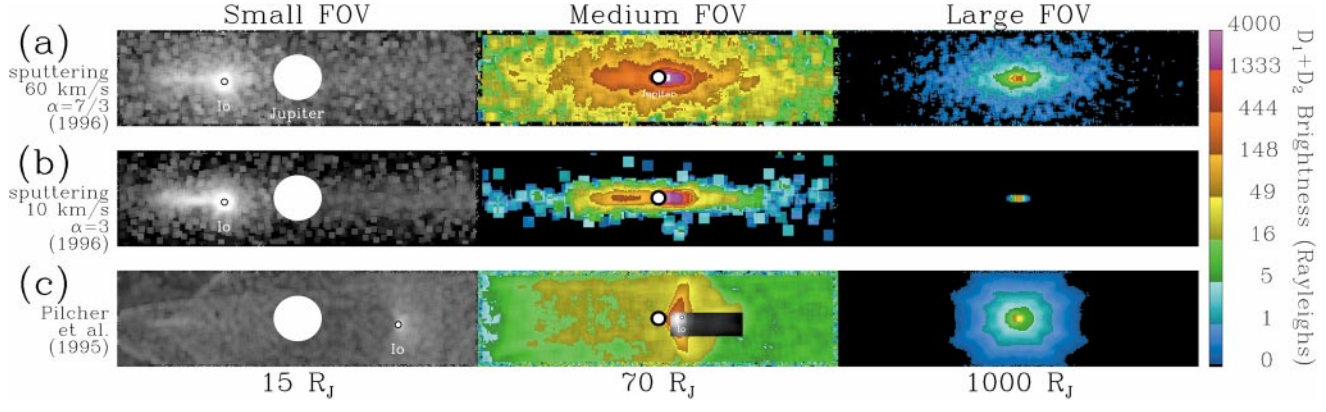

FIG. 6. Images of additional ejection models. The fields of view are 15, 70, and 1000 R_J from left to right. (a) High-speed sputtering ($\alpha = 7/3$ and $v_{plasma} = 60$ km/s) for the geometries of the 1996 data. (b) Low-speed sputtering ($\alpha = 3$ and $v_{plasma} = 10$ km/s) for 1996 data geometries. (c) Pilcher *et al*. Directional Feature model for the 1995 data geometries.

(Figs. 4c and 4d). Finally, Figs. 4d and 4e are identical except for the ion lifetime, which is 3 h and 10 h, respectively.

It is not unreasonable to expect the molecular pickup ions in the stream to have a scattered velocity distribution; *in situ* observations by the Galileo spacecraft indicate that a localized ring distribution of heavy molecular pickup ions in the torus produces ion-cyclotron waves (Kivelson *et al*. 1996, Warnecke *et al*. 1997), which should ultimately scatter the ion velocities (Huddleston *et al*. 1997). Given this, and the ability of the scattered distribution models to reproduce the large-scale nebula at high gyrospeeds (Figs. 4d and 4e) and a narrow stream at low gyrospeeds (Fig. 4c), we will simplify our analysis by using only the scattered distribution in the final stream models.

One interesting difference between low- and high-gyrospeed stream models is the total brightness of the nebula; it is dimmer for higher gyrospeeds. This is due to the average speed away from Jupiter and the interplay among ion gyrospeeds, neutral orbital speeds, and ionization by the plasma torus. At low gyrospeeds, ion neutralization produces Na at speeds only slightly higher or lower than the magnetospheric corotation speed of 74 km/s. All of these atoms leave the torus relatively quickly on escape trajectories. For gyrospeeds near 57 km/s, however, some of the Na is liberated at speeds very close to Io's orbital speed ($74 - 57 = 17$ km/s). These atoms not only fail to move out into the nebula but proceed to orbit Jupiter at Io's orbital distance and are quickly reionized by the torus; thus they contribute relatively little to the sodium cloud emission. High-gyrospeed Na liberated at the opposite cyclotron phase travels at nearly twice the corotation speed ($74 + 57 = 131$ km/s), thus leaving the system more quickly and contributing less to the nebula emission than atoms traveling at only 74 km/s.

Pickup ion neutralization: The "stealth stream." The model of Fig. 4e produces a rectangular nebula in the medium and large FOVs that is very similar to several of the data images, and at the same time it yields a stream in the small FOV that is almost invisible compared to other models. This suggests that the absence of an obvious stream feature in small FOV data images is not necessarily indicative of a lack of molecular pickup ion neutralization. Henceforth we refer to the model in Fig. 4e as the "stealth stream"; it figures prominently in our final analysis.

Pickup ion neutralization: The jet. The jet is a narrow cloud which extends from Io in a direction approximately away from Jupiter. Like the stream, the jet is seen only intermittently, and it moves north and south over several hours in a manner corresponding to Io's magnetic longitude (Pilcher *et al*. 1984). Pickup ion neutralization over Io's trailing, antijovian longitudes explains jet observations seen in several data sets (Wilson 1996, Wilson and Schneider 1999, Burger *et al*. 1999); thus this mechanism is a variant of the stream, with ions being neutralized within seconds of their pickup instead of hours. The antijovian location of the source region indicates that the jet is a result of the escape or "rip-off" of Io's ionosphere (Wilson 1996, Wilson and Schneider 1999). We assume in this study that the forward drift speed of the ions when they are neutralized is the same as the pickup speed, since the ions are created and destroyed in nearly the same location. It is uncertain at this point whether the parent ions are Na^+ ions that charge exchange with Na in the atmosphere or simply the NaX^+ ions of the stream being dissociated near Io by reactions (1a) and (1b) (Wilson 1996, Wilson and Schneider 1999).

The free parameters for the jet model are (1) the ejection rate of Na, (2) the pickup speed of the parent ions, and (3) the velocity modification of the pickup ions. These parameters are identical to those of the stream model, except that the pickup ion lifetime is fixed at a much shorter value. Pickup ions are presumably neutralized at all ion cyclotron phases; however, the fast sodium thus created does not escape at all gyrophases, because Io blocks the atoms that are sent toward Jupiter. We therefore save computation time in the model by limiting the ion gyrophases to those most likely to result in escape of Na.

Figure 5 shows four models of the jet for the same geometries as the 1995 data and with a Na ejection rate of 1.5×10^{27} atoms/s. Jet models using a ring distribution (Figs. 5a and 5b) produce a more distinct jet in the small and medium FOVs, a "lumpy" nebula in the medium FOV, and a distinctly X-shaped nebula in the large FOVs. The scattered distribution, on the other hand, produces a more symmetric and smoother nebula in the medium and large FOVs, more like what is seen in the data.

This adaptation of the stream model to the jet by Wilson (1996) and Wilson and Schneider (1999) was originally inspired by images and spectra of Pilcher *et al*. (1984), Goldberg *et al*. (1984), and Schneider (1988), as well as the groundbreaking realization by Schneider (1988) that charge exchange of pickup ions at Io could lead to narrowly directed ejection of fast neutrals. The ability of our model to reproduce the long ($\sim 10\ R_J$) jet seen in the 1995 medium FOV of Fig. 2, as well as the Galileo image of the jet near Io (Burger *et al*. 1999), provides further evidence of its validity. However, a full comparison between the data images and the jet models reveals that the jet process is probably never the only Na ejection process at work. Although the small FOV image in 1995 (Fig. 2) shows only a jet, none of the jet models can entirely match all three FOVs from that or any other year. The model in Fig. 5c comes close with a straight jet in the small FOV and a smooth, symmetric nebula in the large FOV. However, it produces a distinctly asymmetric nebula in the medium FOV, contrary to the data. Something similar to the stealth stream model of Fig. 4e must be occurring along with the jet in 1995 to account for the inner nebula.

Banana cloud and atmospheric sputtering. Atmospheric sputtering is a process in which plasma torus ions impact neutrals in Io's atmosphere, initiating a cascade of collisions which can ultimately eject several atoms and molecules from the atmosphere for each incident ion (Johnson 1994b). Smyth and Combi (1988) have modeled the near-Io clouds formed by atmospheric sputtering ejection in great detail, demonstrating that isotropic

ejection from Io by this process can produce the banana cloud. However, the contribution of this process to the nebula has until now been ignored in interpretations of nebula images. Here we use our model to test isotropic ejection from Io using the sputtering velocity distribution of Smyth and Combi.

Along with the ejection rate, the only other free parameter in our atmospheric sputtering model is the speed distribution of the Na atoms escaping from Io. Smyth and Combi (1988) calculated a theoretical form of the speed distribution resulting from atmospheric sputtering. The nonnormalized flux of atoms as a function of speed is given by

$$\bar{\phi}(v;\alpha, v_b, v_M) = \frac{1}{v_b}\left(\frac{v}{v_b}\right)^3\left(\frac{v_b^2}{v^2+v_b^2}\right)^{\alpha} \times\left[1-\left(\frac{v^2+v_b^2}{v_M^2}\right)^{1/2}\right], \qquad (2)$$

where v is the ejection speed of the atom, α is a parameter affecting the overall shape of the speed distribution, v_b is a "low cutoff" speed to prevent the slowest nonescaping atoms from dominating the distribution, and v_M is equal to $[2M/(M+m)]v_{\text{Plasma}}$, the maximum velocity an atom of mass m can obtain in a single elastic collision with an ion of mass M traveling at v_{Plasma} (Smyth and Combi 1988). Smyth and Combi have considered α values of $7/3$ and 3, and we use these values for our models. For each model, we use a speed distribution which is a combination of the distribution resulting from sulfur ions colliding with Na and the distribution resulting from oxygen ions colliding with Na. In their studies of the Na speed distribution near Io, Smyth and Combi assumed that ions hit Io's atmosphere at the relative magnetospheric corotation speed of 57 km/s. However, given the evidence for slowed plasma near Io in images of the stream (Schneider *et al*. 1991, Wilson and Schneider 1994), from *in situ* data (e.g., Frank *et al*. 1996), and from theoretical models of plasma flow past Io (e.g., Linker *et al*. 1991), we generate models with relative plasma speeds ranging from 10 (slowed) to 60 km/s (corotation speed).

For completeness, it is worth noting some subtle effects on the banana cloud which we are ignoring in our model. First, the torus is not symmetric around all longitudes of Jupiter. The radial distances and values of the peak plasma density and temperature are functions of both magnetic longitude and local time (Schneider and Trauger 1995), so the ionization rates of Na vary from the average rates we assume in our model. Second, a small fraction (10%) of the Na atoms in the banana are scattered by elastic collisions with torus ions before they are ionized (Brown *et al*. 1983, Schneider *et al*. 1989, and references therein). We ignore these collisions, which means that the banana cloud is not actually as narrow as our model would suggest.

In our model, the form of the speed distribution resulting from atmospheric sputtering has a strong influence on the appearance of the resulting sodium cloud. Figures 6a and 6b show two models of atmospheric sputtering for the geometries of the 1996 data with ejection rates of 6×10^{26} atoms/s. The model in Fig. 6a has the highest overall speed range of the models we tested, with $\alpha = 7/3$ and $v_{\text{Plasma}} = 60$ km/s, while the model in Fig. 6b has the lowest speeds, with $\alpha = 3$ and $v_{\text{Plasma}} = 10$ km/s.

We can draw two important conclusions from the atmospheric sputtering models in Fig. 6. First, any speed distribution we choose in the range bracketed by Figs. 6a and 6b produces the banana cloud in the small FOV. Second, higher speed distributions of atmospheric sputtering can contribute to the sodium nebula. Determining the exact sputtering speed distribution from the data is beyond the scope of this paper, so the extent to which sputtering actually contributes to the nebula remains an open issue.

Even with an uncertain contribution of atmospheric sputtering to the nebula and the approximations made in our model, some interpretations can be made. The small FOV data from 1992, 1994, and 1996 show only the banana cloud with little or no evidence of the stream or jet; and the corresponding large FOV images each show a nebula which our high-speed sputtering model has some success in reproducing. We will assume that pickup processes account for any portion of the distant sodium emission for which the sputtering model alone cannot account. The stealth stream is a particularly good candidate for making the nebula since it produces little or no obvious feature in the small FOV. We model the years which show only the banana cloud in the small FOV by combining the stealth stream and sputtering in amounts which are as consistent as possible with all three FOVs. If the true sputtering distribution is actually faster than the fastest sputtering model here, then a smaller total sputtering rate is capable of producing the same nebula, and we are overestimating the ejection rates from both the stealth stream and sputtering in those years.

Earlier "Directional Feature" model. Pilcher *et al*. (1984) used a different model to explain the jet, or "directional feature" as they referred to it. In their model, Na is ejected from Io's exobase at ~20 km/s and in directions roughly perpendicular to Io's orbital motion. Preferential ionization of the Na either north or south of Io's orbital plane by the tilted, rotating plasma torus results in a broad cloud feature which extends slightly in the opposite direction; thus the cloud feature moves north and south in phase with Io's magnetic longitude.

The Pilcher *et al*. model does not compare favorably with our data. Figure 6c shows model images using an escape rate of 4×10^{26} atoms/s for the geometries of the 1995 data where a jet is seen in both the small and medium FOVs. The model fails to reproduce the jet at either spatial scale, and it suffers the same problem as the thermal charge exchange model in the medium and large FOVs: a high-speed source localized at Io always results in an asymmetric inner nebula. The stripes in the large FOV model image result from the perfectly monoenergetic source in the model and should therefore not be taken literally; we are concerned here with the large-scale morphology of the cloud. It should be noted that atmospheric sputtering

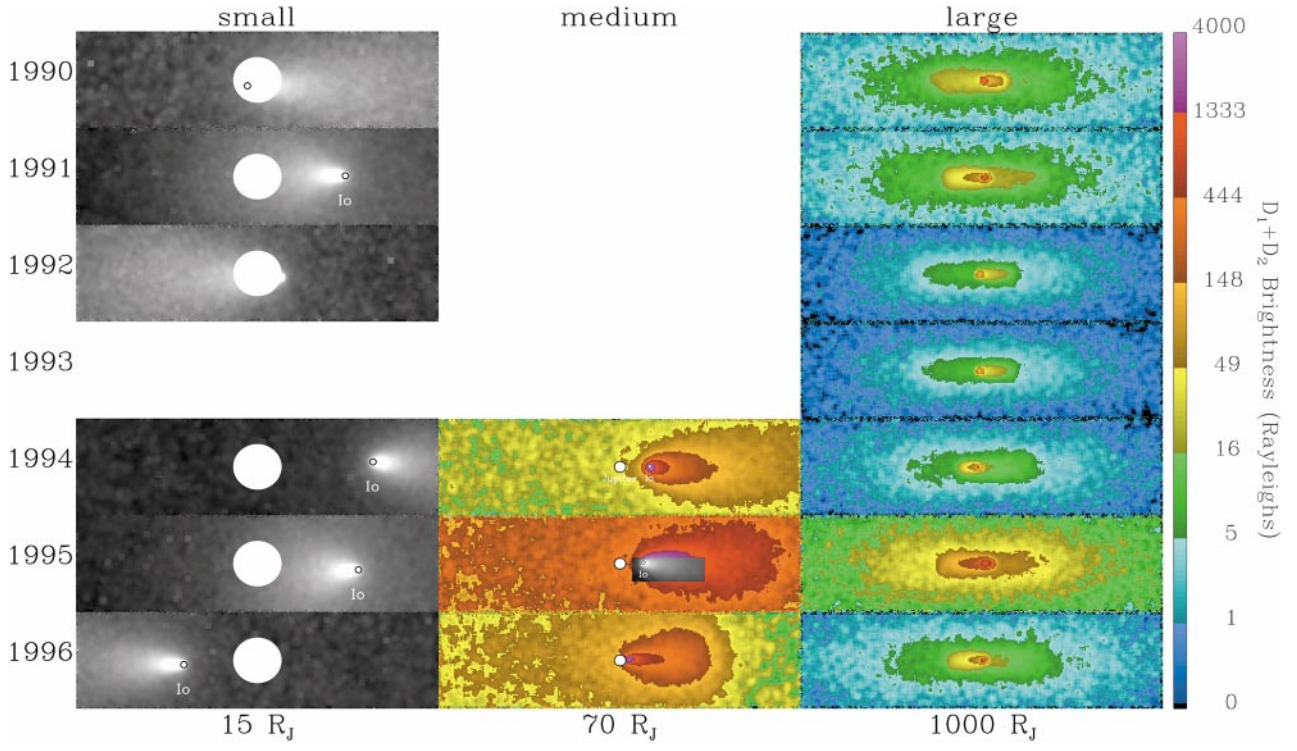

FIG. 7. Thermal exospheric charge exchange models for the complete data set. The fields of view are 15, 70, and 1000 R_J from left to right. Model parameters are given in Table V. These models are meant to derive upper limits to the thermal charge exchange process from the medium and large FOVs; they do not include other features seen in the small and medium FOVs.

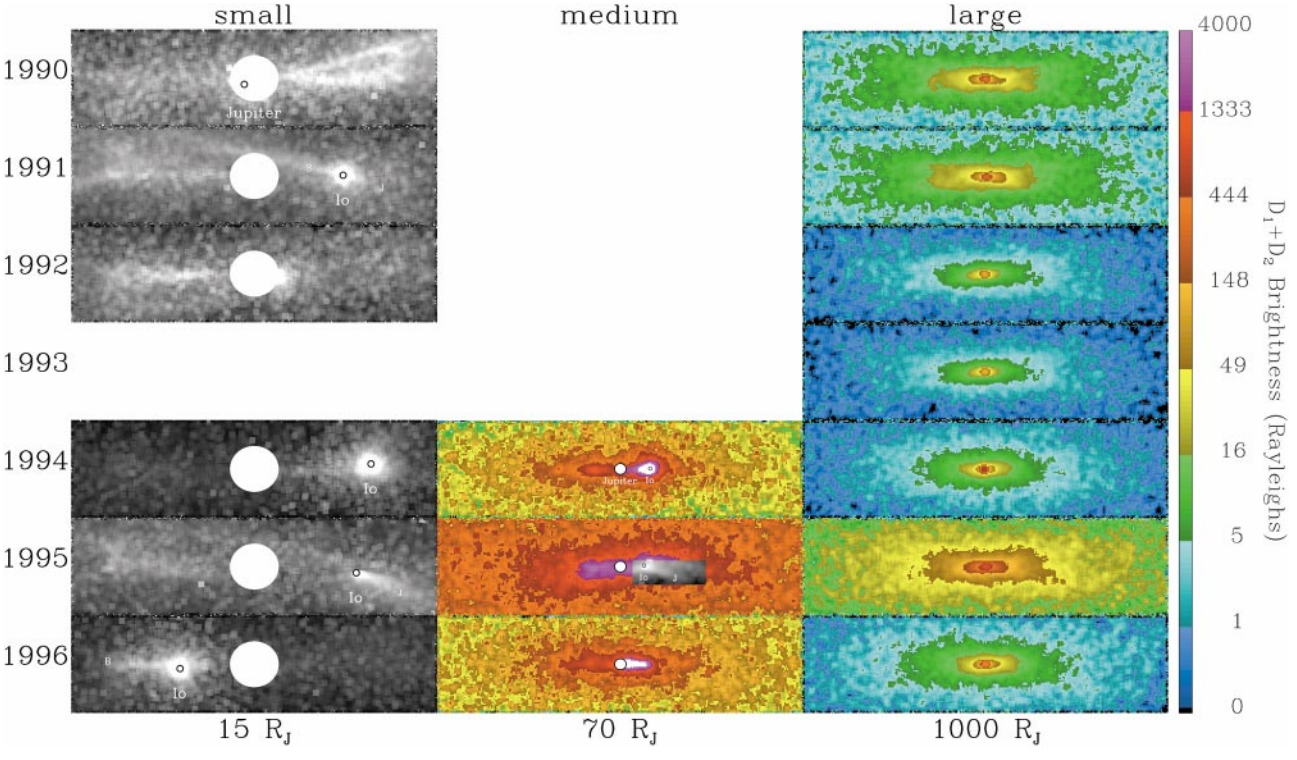

FIG. 8. Final combined models of sputtering, stream, and jet processes for complete data set. The fields of view are 15, 70, and 1000 R_J from left to right. The banana cloud ('B'), jet ('J'), and stream ('S') are labeled in the small FOV images. Model parameters are given in Table VI.

produces the Pilcher *et al*. source distribution as a small part of a much broader and mostly slower velocity distribution. However, Pilcher *et al*. required a limited range of speeds close to 20 km/s to produce a north–south directional effect in their model, and they found that ejection speeds which are too low resulted in directionality opposite to the observed jet. Given the model's inability to produce the jet here, and the lower ejection speeds from atmospheric sputtering, we amplify the conclusion of Wilson and Schneider (1999) that the Pilcher *et al*. mechanism is not responsible for the jet and that it does not proceed at rates above what would be expected as part of the atmospheric sputtering distribution. We will not include this model in our final analysis of the data.

Exospheric charge exchange "fan." Charge exchange between thermal torus Na^+ ions with Na atoms in Io's exosphere became the paradigm high-speed sodium mechanism when sodium speeds of tens of kilometers per second were first measured spectroscopically (Eviatar *et al*. 1976, Brown and Schneider 1981):

$$Na^+_{torus} + Na_{exosphere} \rightarrow Na^* + Na^+_{pickup}. \quad (3)$$

This mechanism was assumed to be the source of the large FOV nebula upon its discovery (Mendillo *et al*. 1990, Smyth 1992), although simple models produced an obvious spiral-arm structure and east–west asymmetry which is not seen in data images. Refinements of the model used a two-component velocity distribution to smear out the spiral-arm structure and more closely reproduce the observed nebula (Smyth and Combi 1991, Flynn *et al*. 1992, Mendillo *et al*. 1992).

Figure 7 shows models of thermal exospheric charge exchange for each of the data images, and Table V lists the ejection rates used for each year. This model is similar to the two-component model of Smyth and Combi (1991); the plasma temperature is 50 eV, and 1/3 of the plasma flows at 37 km/s while 2/3 flows at the corotation speed of 74 km/s. The rate of Na ejection from Io is the only free parameter for this model, and we adjust it for each year to match the data brightnesses as closely as possible. In the large FOV, the "flaring angle" of the nebula arises from a combination of the plasma drift speed and the thermal velocities of ions in the torus ($T = 50$ eV, giving $v_{avg} = 23$ km/s). The forward velocity is sufficient to eject atoms from the system on nearly straight trajectories, and the thermal velocities of the parent ions cause the daughter atoms to spread out as they leave the system, producing the characteristic shape of the nebula.

TABLE V
Upper Limits for Thermal Charge Exchange Rate

Year	Rate (10^{26} Na atoms/s)
1990	4
1991	4
1992	1.5
1993	1.5
1994	2
1995	15
1996	3

Despite its ability to approximate the Na nebula in the large FOV, thermal exospheric charge exchange is probably not the primary sodium ejection mechanism at Io. On spatial scales of the small FOV, the predicted fan-shaped cloud leading Io has never been identified unambiguously in any images dating back to at least 1980. The medium FOV images of Fig. 7 reveal that thermal charge exchange acting alone is not consistent with the data. The model produces a highly asymmetric cloud that is usually much brighter on one side of Jupiter than the other; but the brightness contours in the medium FOV data images (Fig. 2) show that Na emission is nearly the same on both sides of Jupiter. So, although the two-velocity component model is able to smear the spiral arms in the distant nebula, at smaller spatial scales it still results in highly asymmetric clouds, which are not observed. We therefore treat the model results here as extreme upper limits to the thermal exospheric charge exchange rate.

COMBINED MODELS AND EJECTION RATES

For our final combined models we use the sputtering and pickup ion neutralization models only. We derive Na escape rates from Io for each process and for each set of images by comparing model images with data to match the morphology and brightness of the Na clouds seen in all three FOVs. Given that the stream, the jet, and sputtering all eject sodium into the nebula, there are no unique solutions to the data for any given year. However, since the nebulae of 1990, 1991, and 1995 resemble the stealth stream model so closely, it is most likely that the stream, and not a coincidental combination of other processes, is the dominant mechanism for forming those nebulae. Table VI lists the ejection rates found for each process, and the final model images are shown in Fig. 8. Error estimates include uncertainties in absolute brightness of the data (±20%) and imperfect matches between model and data images.

We obtain Na ejection rates in the 1990 and 1991 data partly by trying to achieve the correct relative brightnesses of stream and banana in the model as seen in the small FOVs. The banana cloud is barely visible in the 1991 image near Jupiter, but we assume that it existed on that night (Feb. 6, 1991) as it was seen more clearly with the better geometries on several previous nights (Jan. 31, Feb. 2, 3, 5; Wilson and Schneider 1994). The 1991 image we use here was chosen to be as close as possible in time to the large FOV image taken on Feb. 7 and unfortunately is a poor viewing angle for the banana cloud.

The 1992, 1994, and 1996 data are modeled by first using the stealth stream to produce the nebula and then adding as much atmospheric sputtering as possible while remaining consistent with the small and medium FOVs. There are no small or medium

TABLE VI
Na Ejection Rates: Sputtering and Pickup Ion Neutralization[a]

Year	Atmospheric sputtering: "Banana" & nebula	Na^+_{pickup} or NaX^+_{pickup} neutralization: Stealth stream & nebula	Other stream	Jet	Total
1990	2.0 ± 0.7	4.5 ± 1.6	1.2 ± 0.4[b]	($\leq$1)	7.7 ± 1.8
1991	1.5 ± 1.0	4.0 ± 1.4	2.0 ± 0.7[c]	0.05 ± 0.02[c]	7.6 ± 1.6
1992	1.2 ± 0.6	2.0 ± 1.0	($<$0.3)[b]	($\leq$0.5)	3.2 ± 1.2
1993	0.0–3.0	1.8 ± 0.7	($\leq$0.5)	($\leq$0.5)	3.3 ± 1.6
1994	8 ± 3	2 ± 1	($<$.5)[b]	($<$.5)	10 ± 3
1995	($\leq$2)	22 ± 8	($<$4)[b]	3 ± 2[d]	25 ± 8
1996	9 ± 3	3 ± 1	($<$.5)[b]	($<$.5)	12 ± 3

[a] In units of 10^{26} Na atoms/s. Values in parentheses indicate upper limit for an undetected process.
[b] Gyrospeed = 10 km/s, or limit for gyrospeed = 10 km/s.
[c] Gyrospeed = 30 km/s.
[d] Combination of gyrospeeds from 10 to 60 km/s.

FOV images for 1993, so we have weaker constraints on rates and processes for that year.

DISCUSSION

Our results, as well as results of earlier work, indicate that the flow of plasma through Io's ionosphere is a significant driver of Io's atmospheric escape. The relatively small molecular ion production rates inferred from earlier stream observations require a total source region population that is many times greater than the exosphere (Wilson and Schneider 1994), and we have found even higher stream production rates here. *In situ* measurements by the Galileo spacecraft have revealed significantly slowed plasma near Io (Frank *et al*. 1996) and a dense ionosphere around it (Hinson *et al*. 1998), suggesting that Io's collisionally thick neutral atmosphere interacts with a significant flux of plasma. Added to these points are the observed lack of the thermal exospheric charge exchange fan in this work and the observed presence of the jet found here and by many other observers (Goldberg *et al*. 1984, Pilcher *et al*. 1984, Schneider 1988, Cremonese *et al*. 1992, Mendillo *et al*. 1997, Burger *et al*. 1999, Takahashi *et al*. 2000). The lack of the exospheric charge exchange fan does not rule out charge exchange between torus ions and atmospheric neutrals. In fact, charge exchange may be an important source of ions for both the stream and the jet, but these reactions must be happening within collisionally thick regions of the atmosphere where the products cannot escape to space on collisionless paths. Neutral products of charge exchange there must collide with other neutrals, initiating sputtering cascades "from below," as suggested by Wilson and Schneider (1999). The ion products of charge exchange there can be energized by pickup, leading to additional energetic charge exchange reactions and sputtering cascades. Those Na^+ and NaX^+ ions which survive to escape out the "top" of the atmosphere do so with pickup energy distributions and produce the jet and the stream.

The total Na ejection rates we find here [(3–25) $\times$ 10^{26} atoms/s] are significantly larger than those found in previous studies, partly because, for the first time, we have considered all cloud features and their corresponding escape processes simultaneously in our model. In previous work, the banana, the narrow stream, the jet, and the nebula have all been modeled separately from different data sets. In addition, earlier nebula modelers (e.g., Smyth and Combi 1991, Flynn *et al*. 1992) underestimated the supply rate in some cases because they did not consider the contribution of atmospheric sputtering, which requires a higher ejection rate than other processes to result in the same nebula brightness. Previous stream models (Wilson and Schneider 1994) lacked electron impact ionization and were therefore unable to accurately reproduce the high-gyrospeed stealth stream; they focused on the narrow, low-gyrospeed component of the stream, thereby leading to underestimates of the supply rate. Assuming the escape of "invisible" Na^+ does not dominate the total loss of Na from Io, then the Na escape rates found here are consistent with accepted Na mixing ratios in the torus ($\sim$3%; Gehrels and Stone 1983, Krimigis and Roelof 1983, Bagenal 1985, 1994) and the total atmospheric escape rate from Io, which is thought to be equivalent to $\sim$few $\times$ 10^{28} atoms/s (Barbosa *et al*. 1983, Smyth 1992, Brown 1994).

Although it was recognized earlier that atmospheric sputtering could contribute to the extended regions of the Na clouds (e.g., Smyth 1992), no images of the large FOV Na nebula have been analyzed in terms of atmospheric sputtering until now. Where the sputtering rate can be quantified, we have found rates of (1.2–9) $\times$ 10^{26} atoms/s, comparable to or higher than rates found in other studies. Smyth and Combi (1988) calculated sputtering rates of (1.7–2.7) $\times$ 10^{26} atoms/s from modeling spectra of the banana cloud, and Smyth and Combi (1997) calculated a sputtering rate of (1.7–2.7) $\times$ 10^{26} atoms/s from emission data that included measurements very close to Io. Cremonese *et al*. (1998) calculated low-speed Na escape rates

of (0.7–2.5) $\times$ 10^{26} atoms/s by modeling high-resolution spectra of the banana cloud. Despite these promising results, some uncertainties remain: (1) the speed distribution in our data is undetermined, (2) our model does not include the subtle effects on the banana cloud, and (3) some of our rates were derived from the noncalibrated small FOV images by comparing the brightness of the banana to the stream.

The stealth stream process, or something that produces a similar Na cloud, may at times be the greatest supplier of Io's Na clouds. If our interpretation here is correct, the stealth stream is composed of high-gyrospeed NaX^+ ions (60 km/s) which are not confined to a ring distribution and which have a lifetime of at least $\sim$10 h. Since longer lifetimes simply result in more uniform nebulae and less visible streams, the actual lifetime could be much longer than the 10-h model used here. We have explained this distributed source with the molecular ion stream process only because we know that the stream occurs from the lower gyrospeed cloud features seen in some data, but it is possible that the stealth stream involves a different process altogether. For instance, recombination of thermal Na^+ ions in the torus could also produce a cloud feature like this if there were a means of recombining them on a time scale shorter than the diffusion time out of the torus. Since thermal Na^+ ions in the torus have lower gyrospeeds (v_{avg} = 23 km/s) than those in the stealth stream model (57 km/s), a smaller ejection rate would suffice to yield the same nebula brightnesses. However, under nominal torus conditions, atomic recombination is too slow by a few orders of magnitude (Brown and Schneider 1981).

Although the presence of NaX^+ is inferred from the $\sim$few-hour ion lifetimes seen in the narrow, low-gyrospeed stream images, we do not know the identity of NaX^+, its production mechanisms, or its efficiency for producing Na_{fast} in the torus. Wilson and Schneider (1999) suggest that ionospheric photochemistry and reactions of impinging torus ions are the two most likely production mechanisms, with electron impact ionization probably being less significant. Wilson and Schneider (1994) assumed that only $\sim$20% of NaX^+ yields Na_{fast}, assuming "X" is some combination of S and O. This would mean that NaX^+ escapes from the ionosphere at five times the rate of Na_{fast} production visible in the stream. If this ratio is correct, and if our interpretation of the stealth stream is correct, then our maximum derived NaX^+ destruction rate of (2.2 $\pm$ 8) $\times$ 10^{27} ions/s in 1995 implies a NaX^+ escape rate of (1.1 $\pm$ .4) $\times$ 10^{28} ions/s, an unreasonably large fraction of the total mass loss rate from Io. This may mean that the actual branching ratio to produce Na_{fast} is closer to 100% or that a yet-to-be identified process is producing Na_{fast} in the torus.

NaCl is now a candidate molecule for the stream, given the discovery of Cl ions in the torus (Küppers and Schneider 2000) and new atmospheric chemistry models that predict the formation of $NaCl^+$ in Io's ionosphere from volcanically outgassed NaCl (Moses *et al*. 2000). Although NaCl is prone to condensing onto dust particles in Io's atmosphere (Moses *et al*. 2000), it is unclear whether or not charged dust grains could account for the observed Na escape rates. Our observations would require $\sim$10–100 kg/s of NaCl escape via dust to substitute for the stealth stream process. This is significantly larger than the estimated dust escape rates of .001 kg/s (Horányi *et al*. 1997) and .006–10 kg/s (Graps *et al*. 2000) that are based on dust detections by the Galileo spacecraft.

The banana cloud and the jet may be indicative of conditions in separate, localized atmospheric regions on Io. The banana cloud is populated mostly from ejection over Io's trailing, subjovian quarter (Smyth and Combi 1988), while low-speed atoms sputtered from the leading longitudes of Io populate the inner nebula beyond Io's orbital distance (Smyth and McElroy 1978, Smyth 1992). Thus, isotropic atmospheric sputtering will populate both of these cloud regions. On the other hand, certain characteristics of the jet indicate that it is produced from only the trailing, antijovian quarter of Io (Wilson and Schneider 1999), the region where sputtering contributes the least to any cloud feature. Changes in the atmospheric abundance over this trailing, antijovian quarter could therefore alter the strength of the jet source relative to sputtered cloud features.

Global properties of Io's atmosphere may affect Na escape rates and are probably more important in this respect than conditions in the torus. Changing volcanic activity may alter the abundance and composition of the atmosphere and therefore the chemical production and loss rates of Na and NaX (e.g., Moses *et al*. 2000). Even assuming a constant atmospheric composition, changes in the ion residence times in the atmosphere may determine whether or not NaX^+ ions recombine before they can escape to the torus to form the stream (e.g., Summers and Strobel 1996). Changes in torus composition and/or electron temperature might affect sputtering rates or reaction rates involving NaX^+ in the torus or at the top of Io's atmosphere, but the only observed correlation between torus conditions and sodium cloud brightness indicates that sodium cloud changes *precede* changes in the torus (Brown and Bouchez 1997), a phenomenon that is inconsistent with atmospheric escape rates being affected by torus conditions.

ESCAPE OF S AND O SPECIES

We seek ultimately to understand the escape of Io's atmosphere as a whole, including the more numerous atomic and molecular species of sulfur (S) and oxygen (O). It is not a simple matter to extrapolate our results for Na to S and O species, and it is beyond the scope of this paper to attempt this in any quantitative manner. However, our results here provide a framework for more rigorous studies of the S and O budget in Io's atmosphere and neutral clouds.

There are probably molecular ion streams of O and S species working at rates that are at least comparable to the NaX^+ stream rates found here, although at most they are expected to represent only several percent of the total mass loss rate from Io. Photochemical models predict that molecular ions of SO_2^+, SO^+, and S_2^+ should form in the ionosphere along with NaX^+

(Summers and Strobel 1996, Moses *et al*. 2000). If molecular ion reactions are responsible for producing NaX^+ (Johnson 1994a), then pickup ions of SO_2^+ and other species must be present at comparable numbers. Indeed, wave signatures of pickup ions with masses close to SO_2 were detected by Galileo near Io (Kivelson *et al*. 1996, Warnecke *et al*. 1997), indicating SO_2^+ pickup rates of $\sim 8 \times 10^{26}$/s.

The escape rates in the S and O jets are more difficult to predict from the corresponding Na escape rate. The jet processes may be peculiar to Na. Most ionospheric models predict that Na^+ is the dominant ion in Io's ionosphere (Kumar 1985, Summers 1985, Summers and Strobel 1996, Moses *et al*. 2000), and escaping Na^+ is one possible source for the jet. On the other hand, the Na jet may be formed by recombination/dissociation of escaping NaX^+ near Io's exobase, meaning that escaping SO_2^+ and other molecular ions could produce jets of O and S. In that case, the ejection rates of O and S by the jet process may be at least comparable to the rates for Na.

Species of S, O, and Na are probably sputtered from the atmosphere at rates proportional to their abundances, with S and O escape rates each being at least an order of magnitude larger than Na (Smyth and Combi 1991, Smyth 1992, Smyth and Marconi 2000). Once they are sputtered into their corresponding "banana clouds," S and O atoms suffer somewhat different fates than Na atoms. Over 90% of the Na atoms in the banana cloud are ultimately ionized by torus electron impact (Smyth and Combi 1988, Schneider *et al*. 1989, and references therein), and once ionized they slowly diffuse out of the system with presumably little contribution to the neutral clouds. On the other hand, $\sim$50% of the S atoms and $\sim$70% of the O atoms orbiting Jupiter at Io's orbital distance are ultimately ionized by charge exchange with thermal and superthermal torus ions of S and O (Schneider *et al*. 1989 and references therein, Smyth and Marconi 2000), with the reaction taking the form

$$\mathrm{Ion_{torus}} + \mathrm{Neutral_{banana}} \rightarrow \mathrm{Neutral_{fast}} + \mathrm{Ion} \qquad (4)$$

(McGrath and Johnson 1989). The newly formed fast neutrals escape from the jovian system at corotation speeds or higher, producing "nebulae" of O and S. Thus, although we have ruled out any significant sodium cloud produced by charge exchange of thermal Na^+ torus ions with Na, this process does occur for S^+ and O^+ torus ions moving through the S and O banana clouds.

ACKNOWLEDGMENTS

We thank Don Hunten for insightful comments which improved this paper. We thank Matthew Burger for assistance with modeling and Robert Sturm for data processing assistance. At Boston University, this work is supported by grants from NASA's Magnetospheric Physics and Planetary Astronomy Programs and by Boston University's Center for Space Physics. M. Mendillo, J. Baumgardner, and J. Wilson are Guest Observers at the McDonald Observatory. At the University of Colorado, this work is supported by grants from NASA's Planetary Astronomy Program. Observations at Apache Point Observatory were made courtesy of New Mexico State University, with assistance by Charles Walter.

REFERENCES

Bagenal, F. 1985. Plasma conditions inside Io's orbit: Voyager measurements. *J. Geophys. Res.* **90**, 311–324.

Begenal, F. 1994. Empirical model of the Io plasma torus: Voyager measurements. *J. Geophys. Res.* **99**, 11043–11062.

Barbosa, D. D., F. V. Coroniti, and A. Eviatar 1983. Coulomb thermal properties and stability of the Io plasma torus. *Astrophys. J.* **274**, 429–442.

Baumgardner, J., B. Flynn, and M. Mendillo 1993. Monochromatic imaging instrumentation for applications in aeronomy of the Earth and planets. *Opt. Eng.* **32**, 3028–3032.

Brown, M. E. 1994. Observations of mass loading in the Io plasma torus. *Geophys. Res. Lett.* **21**, 847–850.

Brown, M. E., and A. H. Bouchez 1997. The response of Jupiter's magnetosphere to a volcanic outburst on Io. *Science* **278**, 268–271.

Brown, R. A., and N. M. Schneider 1981. Sodium remote from Io. *Icarus* **48**, 519–535.

Brown, R. A., C. B. Pilcher, and D. F. Strobel 1983. Spectrophotometric studies of the Io torus. In *Physics of the Jovian Magnetosphere* (A. J. Dessler, Ed.), pp. 197–225. Cambridge Univ. Press, New York.

Burger, M. H., N. M. Schneider, and J. K. Wilson 1999. Galileo's close-up view of the Io sodium jet. *Geophys. Res. Lett.* **26**, 3333–3336.

Combi, M. R., M. A. DiSanti, and U. Fink 1997. The spatial distribution on gaseous atomic sodium in the comae of comets: Evidence for direct nucleus and extended plasma sources. *Icarus* **130**, 336–354.

Cremonese, G., N. Thomas, C. Barbieri, and C. Perneshele 1992. High resolution spectra of Io's neutral sodium cloud. *Astron. Astrophys.* **256**, 286–298.

Cremonese, G., H. Boehnhardt, J. Crovisier, A. Fitzsimmons, M. Fulle, J. Licandro, D. Pollacco, H. Rauer, G. P. Tozzi, and R. M. West 1997. Neutral sodium from Comet Hale-Bopp: A third type of tail. *Astrophys. J.* **490**, L119–L202.

Cremonese, G., F. Marzari, N. Eccli, and G. Corrain 1998. The Io sodium cloud: Comparison between observations and numerical models. *Icarus* **131**, 138–151.

Eviatar, A., Y. Mekler, and F. V. Coroniti 1976. Jovian sodium plasma. *Astrophys. J.* **205**, 622–633.

Flynn, B. 1993. Oscillating ion streamline model of Jupiter's neutral sodium nebula. *Adv. Space Res.* **13**, 325–330.

Flynn, B., M. Mendillo, and J. Baumgardner 1992. Observations and modeling of the jovian remote neutral sodium emissions. *Icarus* **99**, 115–130.

Flynn, B., M. Mendillo, and J. Baumgardner 1994. The jovian sodium nebula: Two years of ground-based observations. *J. Geophys. Res.* **99**, 8403–8409.

Frank, L., W. Paterson, K. Ackerson, V. Vasyliunas, F. Coroniti, and S. Bolton 1996. Plasma observations at Io with the Galileo spacecraft. *Science* **274**, 394–395.

Gehrels, N., and E. C. Stone 1983. Energetic oxygen and sulfur ions in the jovian magnetosphere and their contribution to the auroral excitation. *J. Geophys. Res.* **88**, 5537–5550.

Goldberg, B. A., G. W. Garneau, and S. K. LaVoie 1984. Io's sodium cloud. *Science* **226**, 512–516.

Graps, A. L., E. Grün, H. Svedhem, H. Krüger, M. Horányi, A. Heck, and S. Lammers 2000. Io as a source of the jovian dust streams. *Nature* **405**, 48–50.

Hinson, D. P., A. J. Kliore, F. M. Flasar, J. D. Twicken, P. J. Schinder, and R. G. Herrera 1998. Galileo radio occultation measurements of Io's ionosphere and plasma wake. *J. Geophys. Res.* **103**, 29343–29357.

Horányi, M., E. Grün, and A. Heck 1997. Modeling the Galileo dust measurements at Jupiter. *Geophys. Res. Lett.* **24**, 2175–2178.

Huddleston, D. E., R. J. Strangeway, J. Warnecke, C. T. Russell, M. G. Kivelson, and F. Bagenal 1997. Ion cyclotron waves in the Io torus during the Galileo

encounter: Warm plasma dispersion analysis. *Geophys. Res. Lett.* **24**, 2143–2146.

Huebner, W. F., J. J. Keady, and S. P. Lyon 1992. Solar photo rates for planetary atmospheres and atmospheric pollutants. *Astrophys. Space Sci.* **195**, 1–294.

Johnson, R. E. 1994a. Formation of Na-containing molecular ions at Io. *Icarus* **111**, 65–72.

Johnson, R. E. 1994b. Plasma-induced sputtering of an atmosphere. *Space Sci. Rev.* **69**, 215–253.

Kivelson, M. G., K. K. Khurana, R. J. Walker, J. Warnecke, C. T. Russell, J. A. Linker, D. J. Southwood, and C. Polansky 1996. Io's interaction with the plasma torus: Galileo magnetometer report. *Science* **274**, 396–398.

Krimigis, S. M., and E. C. Roelof 1983. Low-energy particle population. In *Physics of the Jovian Magnetosphere* (A. J. Dessler, Ed.), pp. 106–156. Cambridge Univ. Press, New York.

Kumar, S. 1985. The SO_2 atmosphere and ionosphere of Io: Ion chemistry, atmospheric escape, and models corresponding to the Pioneer 10 radio occultation measurements. *Icarus* **61**, 101–123.

Küppers, M., and N. M. Schneider 2000. Discovery of chlorine in the Io torus. *Geophys. Res. Lett.* **27**, 513–516.

Linker, J. A., M. G. Kivelson, and R. J. Walker, 1991. A three dimensional MHD simulation of plasma flow past Io. *J. Geophys. Res.* **96**, 21037–21053.

McGrath, M. A., and R. E. Johnson 1989. Charge exchange cross sections for the Io plasma torus. *J. Geophys. Res.* **94**, 2677–2683.

Mendillo, M., J. Baumgardner, B. Flynn, and W. J. Hughes 1990. The extended sodium nebula of Jupiter. *Nature* **348**, 312–314.

Mendillo, M., B. Flynn, and J. Baumgardner 1992. Imaging observations of Jupiter's sodium magneto-nebula during the Ulysses encounter. *Science* **257**, 1510–1512.

Mendillo, M., J. Wilson, J. Baumgardner, and N. Schneider 1997. Groundbased remote sensing of energetic neutral atoms in Jupiter's magnetosphere. In *The Three Galileos: The Man, The Spacecraft, The Telescope* (J. Rahe, C. Barbieri, T. Johnson, and A. Sohus, Eds.), pp. 411–420. Kluwer Academic Publishers, Dordrecht, The Netherlands.

Moses, J. I., M. Yu Zolotov, and B. Fegley, Jr. 2000. Photochemistry of a volcanically driven atmosphere on Io. *Bull.—Am. Astron. Soc.* **32**, 1057–1058.

Pilcher, C. B., W. H. Smyth, M. R. Combi, and J. H. Fertel 1984. Io's sodium directional features: Evidence for a magnetospheric-wind-driven gas escape mechanism. *Astrophys. J.* **287**, 421–444.

Schneider, N. M. 1988. *Sodium in Io's Extended Atmosphere*. Ph.D. thesis, University of Arizona, Tucson.

Schneider, N. M., and J. T. Trauger 1995. The structure of the Io torus. *Astrophys. J.* **450**, 450–462.

Schneider, N. M., W. H. Smyth, and M. A. McGrath 1989. Io's atmosphere and neutral clouds. In *Time-Variable Phenomena in the Jovian System* (M. J. S. Belton, R. A. West, and J. Rahe, Eds.), pp. 75–99. National Aeronautics and Space Administration, Washington, DC.

Schneider, N. M., J. T. Trauger, J. K. Wilson, D. I. Brown, R. W. Evans, and D. E. Shemansky 1991. Molecular origin of Io's fast sodium. *Science* **253**, 1394–1397.

Smyth, W. H. 1992. Neutral cloud distribution in the jovian system. *Adv. Space Res.* **12**, 8337–8346.

Smyth, W. H., and M. R. Combi 1988. A general model for Io's neutral gas clouds. II. Application to the sodium cloud. *Astrophys. J.* **328**, 888–918.

Smyth, W. H., and M. R. Combi 1991. The sodium zenocorona. *J. Geophys. Res.* **96**, 22711–22727.

Smyth, W. H., and M. R. Combi 1997. Io's sodium corona and spatially extended cloud: A consistent flux speed distribution. *Icarus* **126**, 58–77.

Smyth, W. H., and M. K. Marconi 2000. Io's oxygen source: Determination from ground-based observations and implications for the plasma torus. *J. Geophys. Res.* **105**, 7783–7792.

Smyth, W. H., and M. B. McElroy 1978. Io's sodium cloud: Comparison of models and two dimensional images. *Astrophys. J.* **226**, 336–346.

Spencer, J. R., and N. M. Schneider 1996. Io on the eve of the Galileo mission. *Annu. Rev. Earth Planet. Sci.* **24**, 125–190.

Summers, M. E. 1985. *Theoretical Studies of Io's Atmosphere*. Ph.D. thesis, California Institute of Technology, Pasadena.

Summers, M. E., and D. F. Strobel 1996. Photochemistry and vertical transport in Io's atmosphere and ionosphere. *Icarus* **120**, 290–316.

Takahashi, S., H. Misawa, H. Nozawa, A. Morioka, R. Sood, S. Okano, and K. Yumoto 2000. Distribution of sodium cloud near Io and in the inner jovian magnetosphere. *Adv. Space Res.* **26**, 1529–1532.

Warnecke, J., M. G. Kivelson, K. K. Khurana, D. E. Huddelston, and C. T. Russell 1997. Ion cyclotron waves observed at Galileo's Io encounter: Implications for neutral cloud distribution and plasma composition. *Geophys. Res. Lett.* **24**, 2139–2142.

Wilson, J. K. 1996. *Io's Fast Sodium Clouds and the Escape of Io's Ionosphere*. Ph.D. thesis, University of Colorado, Boulder.

Wilson, J. K., and N. M. Schneider 1994. Io's fast sodium: Implications for molecular and atomic atmospheric escape. *Icarus* **111**, 31–44.

Wilson, J. K., and N. M. Schneider 1999. Io's sodium directional feature: Evidence for ionospheric escape. *J. Geophys. Res.* **104**, 16567–16583.